# From Chiral Islands to Smectic Layers: A Computational Journey Across Sexithiophene Morphologies on $C_{60}$

*Gabriele D'Avino, Luca Muccioli, and Claudio Zannoni**

**A theoretical investigation of the molecular organization at a sexithiophene (T6)-$C_{60}$ fullerene planar heterojunction, based on atomistic molecular dynamics, is presented, in which the effect of two different sample preparation processes on the resulting interface morphology is explored. First, the landing of T6 on $C_{60}$(001) substrate is considered, which leads to crystalline layers of standing and tilted molecules, in accordance with experiments. The observation and the quantitative characterization of the nucleation and growth provide detailed insights on this out-of-equilibrium process, including the establishment of an epitaxial relationship between the substrate and the interfacial T6 layer, and the spontaneous formation of defective islands, characterized by chiral edges, during the growth of the second and third layers. It is then shown that molecular orientations can be radically changed upon annealing at 600 K, at which T6 forms a smectic phase with planar alignment, whose layers are perpendicular to the interface. The interfacial T6 morphologies are then analyzed in detail at room temperature and compared to the known bulk polymorphs.**

## 1. Introduction

A key element of any organic solar cell (OSC)[1,2] is the interface between electron donor (D) and acceptor (A) materials where tightly bound charge pairs, originated from the decay of photogenerated excitons, dissociate. If this process can successfully compete with charge recombination, the separated charges can travel towards their respective electrodes performing a necessary step towards achieving conversion of solar light in electricity. The evaluation of the different competing electronic processes taking place at the DA interface is far from obvious[3–6] and its results can even be counterintuitive[7–9] because they strongly depend on the detailed knowledge of the donor and acceptor molecular organization,[9–12] as can now be achieved in favorable cases by atomistic molecular dynamics (MD) simulations.[9,13–16]

Further development in improving the performance of OSC requires a deeper knowledge and ability to control the molecular organization at the interface between the materials playing the role of electron donor and acceptor. Important factors are the choice of donors and acceptors chemical nature, their morphology and the type of heterojunction, which currently consists of either a planar interface between two thin layers of donor and acceptor (bilayer cell,[17] possibly replicated) tandem cells,[18,19] or an interpenetrated bicontinuous arrangement where the D, A materials are microsegregated inside a single photoactive layer (bulk heterojunction or BHJ).[20,21] The orientation of donor and acceptor molecules at their interface and in particular the possibility of, say, "face–face" instead of "edge on" disposition of the respective aromatic moieties is of great importance for bilayer, as well as for BHJ cell performances.[22,23]

As far as materials are concerned, both small molecules and polymers have and are being used. In general terms of efficiency polymer based devices, more extensively studied, have shown the best top performance, but small molecule cells are now showing similar results.[24,25] Small molecules have the advantage of being of a well-defined chemical composition: they can be easily purified and their physical properties can be determined and controlled favoring a better reproducibility of solar cell performance with respect to the batch to batch variations often found in polymers. While chemical composition represents an essential aspect, polymorphism for crystalline materials or more generally the detailed molecular arrangement in space (e.g., the type of mesophase for liquid crystalline materials)[26] plays an important role. For small molecule materials these aspects can be thermodynamically controlled and well defined reaching equilibrium conditions at a certain temperature *T*, pressure *P*, and composition. However molecular organizations can very significantly change in thin nanometric films and, moreover, the film preparation process can be a non-equilibrium one making the final result even more difficult to predict.

Here we wish to investigate the possibility of controlling morphology at a donor- acceptor interface prepared with a physical vapor deposition process, applying a methodology we have recently developed and applied to the deposition of pentacene

Dr. G. D'Avino, Dr. L. Muccioli, Prof. C. Zannoni
Department of Industrial Chemistry "Toso Montanari" and INSTM
University of Bologna
Viale del Risorgimento 4, IT-40136 Bologna, Italy
E-mail: Claudio.Zannoni@unibo.it
Dr. G. D'Avino
Department of Physics
University of Liège
Allée du 6 Août 17, BE-4000 Liège Belgium

**DOI: 10.1002/adfm.201402609**

on $C_{60}$.[27] We have chosen as donor $\alpha$-sexithiophene (T6)[28] and as acceptor fullerene ($C_{60}$) that have the advantage of being relatively simple but also well studied experimentally. T6 has been used since more than twenty years[29] as model system for small molecule organic p-type semiconductor, in particular in organic field effect transistors,[30] and to understand crystal nucleation, growth, and epitaxy.[31] Conversely $C_{60}$ fullerene is a standard choice as n-type semiconductor either used as such in its crystalline form or, more often, functionalized to make it soluble and polar as the widely used PCBM which is most often amorphous. The T6-$C_{60}$ interface has been studied with ultraviolet and X-ray photoelectron spectroscopy to assess Fermi level alignment and the extent of charge transfer,[32–34] as it constitutes a prototypical system for solar cells.[35–37] In addition, it has been shown that the relative weak intermolecular interactions at this interface can be exploited and controlled in order to achieve a variety complex architectures.[38–40]

Some simulations of oligothiophenes-$C_{60}$ have been performed: equilibrium films of T4 on $C_{60}$ have been simulated with atomistic molecular dynamics and their properties compared with the bulk.[14] The molecular organization of $C_{60}$ on a monolayer of T6 adsorbed on an Ag(111) surface has been actually studied elsewhere.[41] We are not aware, anyway, of simulations of the all-important process of film formation, of how this influences the morphology and, more importantly of how this can help in trying to suggest a methodology to obtain the planar alignment of T6 on $C_{60}$, rather than the tilted one that is expected to improve performance.[23] In the following, we shall see that such an alignment should be achievable obtaining planar smectic layers by a suitable sample preparation protocol.

## 2. Vapor Growth of T6 on $C_{60}$(001)

The deposition, nucleation and growth of T6 on $C_{60}$ is simulated with a technique based on atomistic molecular dynamics (MD), reminiscent of the experimental process, and proposed in a recent investigation of the pentacene/$C_{60}$ interface.[27] This scheme, in which one T6 molecule at a time is landed on the $C_{60}$(001) substrate, allows the direct observation of the out-of-equilibrium processes at the growing interface, which is left free to self-organize. In the present study, the vapor growth process is followed up to the formation of three T6 monolayers (MLs), as shown by the final snapshot in **Figure 1**a, for a total time of about 250 ns.

A first overview of the mechanism of growth of T6 on C60(001) is given by the evolution of coverage and average tilt angle (formed by the long molecular axis and the $C_{60}$ plane normal, $\Theta$ in Figure 1b) for each ML, as a function of the number of deposited molecules, shown in Figure 1c,d, respectively. The growth proceeds in a layer-by-layer fashion, and is characterized by a collective reorientation of T6 molecules, that are initially adsorbed flat and then stand-up at higher coverage, similarly to what observed in the simulated vapor growth

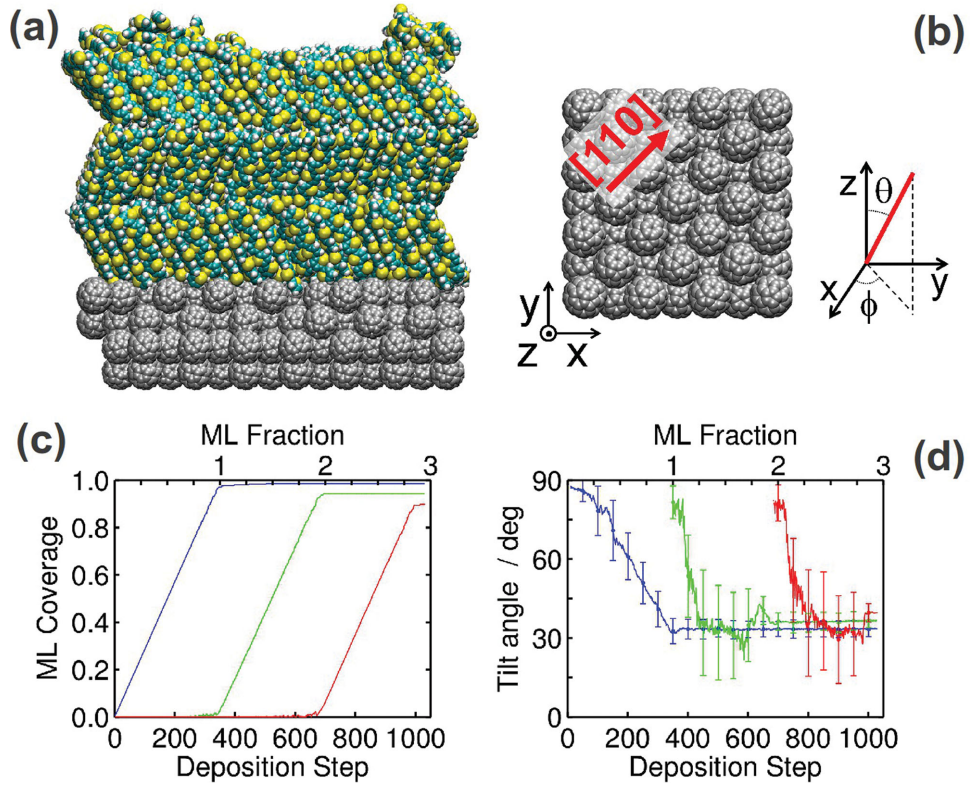


**Figure 1.** a) Final structure obtained after the deposition of 1030 T6 molecules on the $C_{60}$(001) surface, showing that different tilt directions are obtained in each ML. b) Top view of the $C_{60}$(001) surface and definition of the tilt ($\Theta$) and twist or azimuthal ($\phi$) angles. Throughout the paper, molecular orientations are defined by the main inertia axes. c) Fractional coverage in each ML (345 T6 are assumed for a complete ML). d) Tilt angle averaged over the T6 molecules in each ML at different deposition steps, and relative standard deviation (error bars).

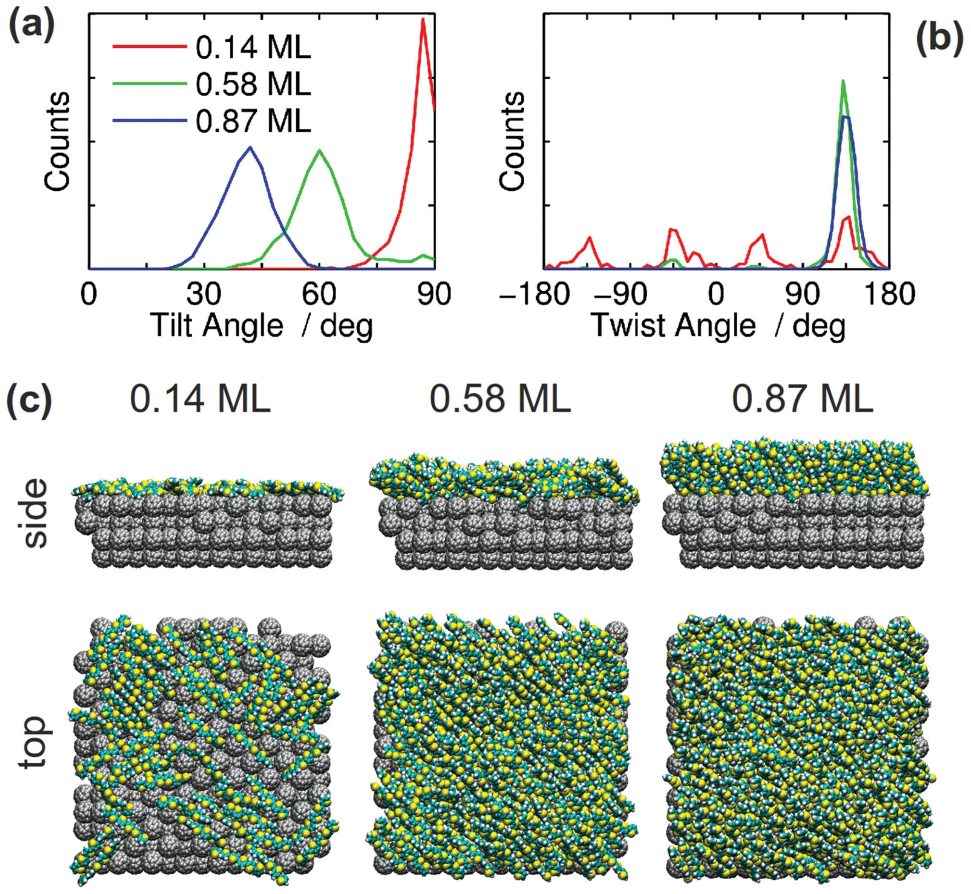


**Figure 2.** Growth of the first T6 ML on $C_{60}$(001). Distributions of a) tilt and b) twist angles of T6 long axis at 0.14 (50 T6), 0.58 (200 T6), and 0.87 (300 T6) ML coverage, and c) corresponding snapshots. The growth of ML1 proceeds through a gradual lying–to–standing reorientation of T6 molecules upon increasing coverage. The azimuthal molecular orientation (twist angle $\phi$) is inherited from the low coverage phase, where T6s are lying parallel to the [$\bar{1}$10] direction of the substrate.

of pentacene on the same substrate,[27] and for T6 on $SiO_2$[42] Going into the details of the growth, already from inspecting Figure 1d, it appears that for ML1 reorientation occurs in a different way with respect to ML2 and ML3. In fact, the average tilt $\Theta$ of ML1 decreases smoothly from 90 to 30 degrees, while for ML2 and ML3 the change of alignment is sharp, though associated with a large spread of values (see error bars in Figure 1d).

To better classify the different stages of the growth, it is useful to follow not only the tilt angle, but also the twist angle defining the direction of molecular tilting with respect to the box $x$ axis, coincident with the $C_{60}$ (100) direction ($\phi$ in Figure 1b). **Figure 2** shows the distributions of $\Theta$ and $\phi$ angles for three representative moments of the growth of ML1, alongside the respective snapshots. At low coverage (0.14 ML) T6 molecules lie flat, maximizing their interaction with the substrate by inserting into the grooves between lines of $C_{60}$ molecules along the ‹110› directions. The molecules do not stay isolated but assemble in domains where T6 long molecular axes are directed along one of the two mutually perpendicular groove directions. This aggregation produces a distribution of twist angles characterized by four peaks (red line in Figure 2b), one for each possible direction. The formation of such domains was not registered for pentacene growth on the same substrate, where the initial wetting layer has no preferred twist orientation,[27] and is instead consistent with photoluminescence and microscopy experiments on $SiO_2$, which proved the existence of layers of flat molecules in the region between standing T6 islands.[42,43]

At increased coverage, the different domains merge into a film with homogeneous molecular orientations, as suggested by the single-peaked distribution of both tilt and twist angles (Figure 2, 0.58 ML). By continuing the deposition until ML completion, whereas the tilt direction remains pinned to the [$\bar{1}$10] direction (Figure 2, 0.87 ML), the average tilt gradually decreases, eventually leading to the formation of a standing layer of crystalline T6. A recent organic molecular beam deposition study provides an experimental confirmation of this result. Radziwon et al. in fact reported the growth of standing T6 layers on $C_{60}$ at high temperature ($T$ > 320 K), with the formation of disordered structures of lying molecules, more suitable for organic solar cell applications, occurring only close to room temperature.[44]

Unlike ML1, the formation of ML2 proceeds via the formation of an initial aggregate of T6 molecules presenting a broad and structure-less distribution of tilt angles, and a quite well defined twist, as shown in **Figure 3** at 1.16 ML coverage. This

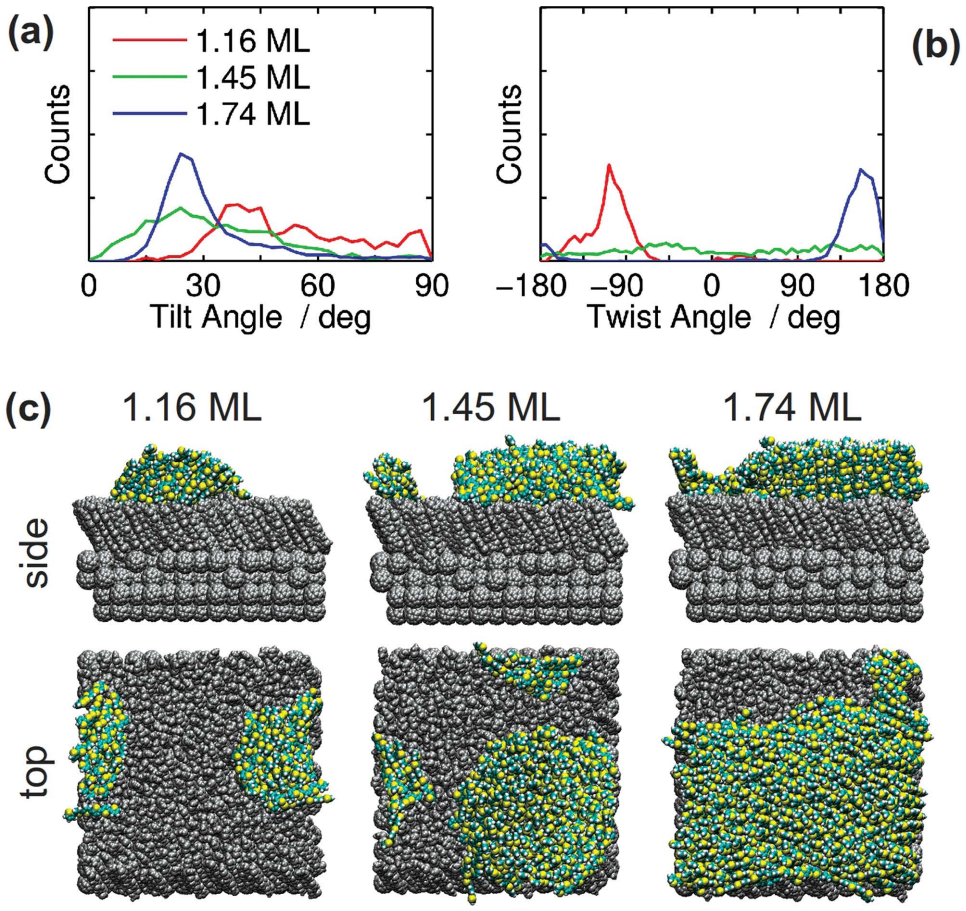


**Figure 3.** Growth of the second T6 ML. Distributions of a) tilt and b) twist angles of T6 long axis at 1.16 (400 T6), 1.45 (500 T6), and 1.74 (600 T6) ML coverage, and c) corresponding snapshots. The growth of ML2 proceeds through the formation of a crystalline island of roughly circular section and defective edges, characterized by a chiral supramolecular organization (see Figure 4). An analogous mechanism is observed for the growth of ML3 (see Figure S5, Supporting Information).

initial aggregate grows in size upon adding new T6 molecules and, when it reaches about 100 T6 units, it transforms into a crystalline island of nearly circular shape (see Figure 3 at 1.45 ML). This nucleus is characterized by a crystalline core, in which standing T6s show a herringbone arrangement, surrounded by a defective edge formed by tilted molecules: the broad distribution of molecular tilts (green line in Figure 3a) presents a maximum just below 30 degrees, belonging to standing molecules in the core, and a tail at larger angles due to molecules at the edges. The distribution of twist angles is even broader (green line in Figure 3c), with in practice all the tilting directions of T6 molecules equally probable.

A closer inspection reveals that actually the island is a chiral supramolecular assembly, in which T6 molecules are locally tangential to the perimeter, leading to a propeller-like structure when observed from the top. This is shown in **Figure 4** for

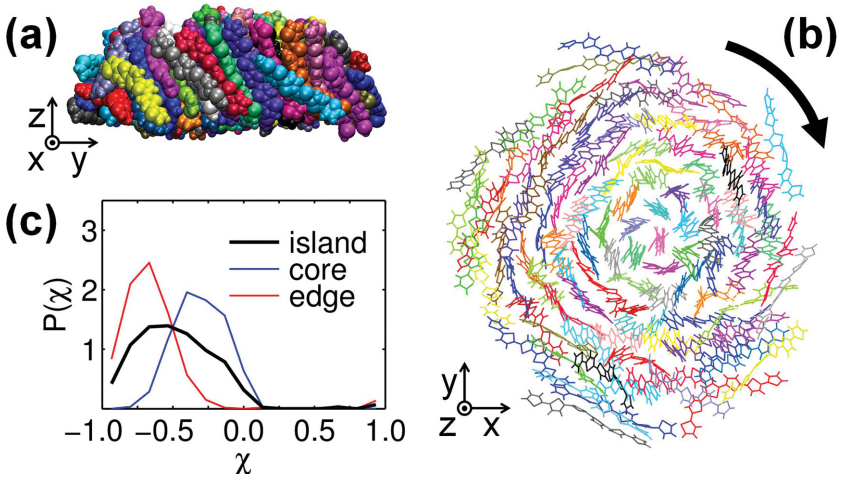


**Figure 4.** a) Side and b) top view of the chiral crystalline island formed by 106 T6 molecules on the T6-ML1 substrate, as obtained from VD simulations at 1.30 ML. For clarity the substrate is omitted and T6 molecules are drawn with different colors. The arrow in (b) shows the direction of molecular tilting. The island chirality is quantified by the asymmetric distribution of the chirality index $\chi$, shown in panel (c). The distributions for the T6 molecules within the core ($r_{\perp}^{i} < 20$ Å), and at the edge of the island are also plotted.

the nucleus formed at 1.30 ML, that is, when the initial disordered aggregate of ML2 starts to self-assemble in a chiral island. In order to quantify the chirality of this object, we computed the distribution of a pseudoscalar chirality index:[45]

$$\chi^i = \hat{n} \cdot \left(\hat{r}_\perp^i \times \hat{u}_+^i\right) \quad (1)$$

Here, $\hat{n}$ defines the axis of the island (vector perpendicular to the plane passing through the island centroid), $\hat{r}_\perp^i$ is the vector pointing from the island axis to the centroid of molecule $i$, and $\hat{u}_+^i$ corresponds to the T6 long axis (the vectors in Equation (1) have all unit length and $\hat{u}_+^i$ is chosen to point in the $z > 0$ direction). The asymmetry of the distribution (thick black line in Figure 4c) demonstrates the chirality of the island, and its negative mean value indicates a left-handed orientation of molecular axes (statistically, right- and left-handed orientations are expected to be equally probable). In Figure 4c we also differentiate the distribution of $\chi$ for the molecules belonging to the core and to the edge of the island. Although the quantitative result depends on the arbitrary definition of the two regions, we find that the outer part is more chiral than the inner one. By depositing more T6 molecules the island grows, expanding its herringbone packed core, and maintaining its chirality at the edges (see Figure S6, Supporting Information). This phase of the growth continues until the island comes into contact with its periodic replica, forming a crystalline ML with well-defined and uniform molecular orientations (see Figure 3, 1.74 ML).

In order to clarify the stability of the chiral island, also in relation to the finite size of our simulation box and to periodic boundary conditions, we performed additional simulations of selected aggregates of the growing second ML on a $2 \times 2$ replica of the substrate (consisting of $C_{60}$ and T6 ML1). Specifically, we considered the chiral aggregate obtained at 1.30 ML and the crystallite at 1.74 ML, formed after the merging of the island with its periodic replica, and simulated them at 300 and 500 K. It turned out that not only the chiral nucleus remains stable on the enlarged substrate, but also the crystallite formed at 1.74 ML rearranges, forming an island with a shape very similar to the former, though the reorganization is much slower at 300 K (initial and final snapshots of these simulations are shown in Figure S4, Supporting Information). This result clearly demonstrates the thermodynamic stability of the crystalline nucleus with disordered and tilted edges, a structure that we suppose to be inherent to the growth of T6 on T6.

We continued the deposition of T6 molecules until the completion of the second and of a third ML, leading to the final structure shown in Figure 1a. The growth of the third ML is qualitatively and quantitatively similar to that of ML2, that is, it proceeds through the formation of a chiral aggregate with disordered edges when about 100 molecules are deposited (Figure S5,S6, Supporting Information), which progressively becomes a true crystalline layer with a tilting direction not correlated with the one of the underlying ML2.

Again this mechanism is at variance with the simulated growth of pentacene in the same thermodynamic conditions: in that case, we did not find such a strong qualitative differences in the growth of ML1 and ML2, and the growing MLs were rather regular also at terrace edges. As a matter of fact, for the case of T6 it turns to be preferable to lose some crystallinity at the terrace edges rather then exposing high energy crystalline surfaces such as (010).[46] It is worth noting that such an effect can only be detected and explored with MD simulations of the growth, which can take into account thermal and structural disorder and kinetic effects, while other, more refined calculations on crystal energetics and structure[47,48] are limited to perfect crystal shapes.

The simulated deposition process seems to produce different, and apparently uncorrelated, molecular orientations in the different layers, that is, a so-called turbostratic structure. This may appear unrealistic, if one considers that the known bulk–phase crystalline polymorphs of unsubstituted oligothiophenes are formed by synclinic layers.[29] However several experimental observations showed that interlayer defects of similar nature may occur in thin molecular films.[49–51] For instance, Campione and co-workers[52] showed that the homoepitaxy of T6 is reduced by increasing temperature, at which even needles of lying molecules can form, indicating that the differences in free energy between the possible orientations are small, as well acknowledged for organic-organic epitaxy.[31,53,54] Interestingly, in reference [52] it was also observed a roughening at (100) terrace edges upon increasing temperature, which was attributed to desorption, but that in the light of the present results it could be also related to the peculiar shape of islands, as discussed above. Indications of a reduced interlayer correlation in T6 films grown on $SiO_2$ are also provided by Raman scattering measurements, in which lattice phonons polarized in the direction perpendicular to molecular layers are not found for thicknesses lower than 10 ML, [50] while conversely grazing incidence X-ray experiments showed that a layered structure still exists.[49]

It is finally worth noting that, despite the absence of epitaxy between the T6 MLs, the standing T6/$C_{60}$ interface produced by vapor deposition may be suitable for devices such as ambipolar field effect transistors, as charge transport is nearly two-dimensional and occurring within the first two monolayers.[30]

## 3. High Temperature Annealing of the T6/$C_{60}$(001) Interface

Besides the two well-known crystal phases, T6 also exhibits at least one liquid crystal (LC) phase above 570 K, as revealed by a few experimental studies carried out in the '90s,[55,56] and recently "rediscovered" by our group with computer simulations.[28] The tunability of the molecular alignment with surfaces, magnetic and electric fields offered by such phases can be in principle exploited to control the morphology of the semiconductor. Indeed, although in the specific case of T6 the crystal-LC phase transition occurs at high temperature, posing severe difficulties to practical applications, other similar materials, such as phenyl-thienyl all-aromatic co-oligomers,[57] or other alkyl substituted aromatic compounds,[58,59] present similar phases at more manageable temperatures. Conversely, the high temperatures of T6 LC phases are not an issue in computer simulations, therefore here, as a proof of principle, we could investigate the behavior of liquid crystalline T6 on the $C_{60}$(001) surface without encountering any technical difficulty.

Since mesophases of rod-like molecules typically show a planar alignment on regular surfaces,[60,61] our aim was to explore the opportunities offered by high temperature annealing for producing an interface more suitable for solar cell applications than the one obtained by vapor deposition, namely one with T6 layers parallel to the $C_{60}$ surface.

A preliminary simulation, performed on the vapor-deposited sample in Figure 1a at 600 K, confirmed that also liquid T6 prefers a planar alignment on the $C_{60}$ surface. We therefore proceeded with constructing an amorphous T6 film wafered between two flat $C_{60}$ surfaces, that is, a situation similar to what may locally occur in bulk heterojunction solar cells—and equilibrated in the NpT ensemble at 600 K and 1 atm (see Experimental Section for details). The choice of a NpT simulation is aimed at avoiding the effect of the interface with vacuum, that typically induces a homeotropic alignment on rod-like mesogens, and may propagate for some nanometers inside the sample.[60,61] Before discussing the results, it is worth recalling that, with the force field used here, melting from the crystal to a layered LC phase (smectic A) occurs at 580 K for bulk samples, and it is followed by the transition to a nematic phase at 610 K and finally to the isotropic liquid at 670 K.[28]

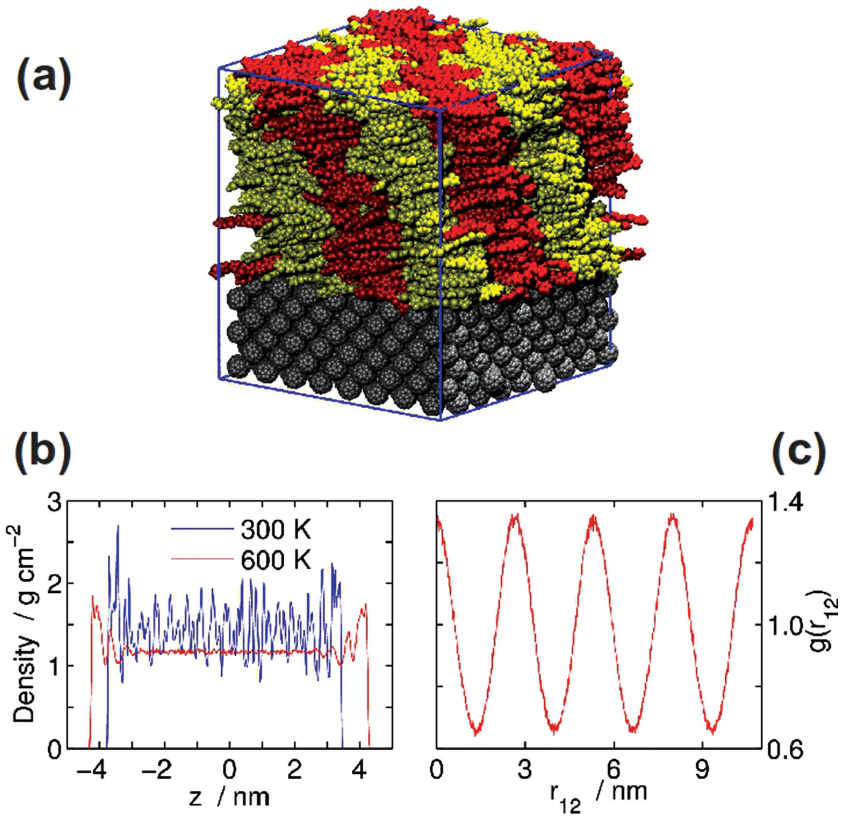


**Figure 5.** Physical properties of the sample annealed at 600 K, shown in panel (a) with T6 molecules belonging to different layers alternatively colored in yellow and red. b) T6 density as a function of the vertical position z, normal to the fullerene surface, plotted at $T = 600$ (red line) and 300 K (blue line). c) Linear pair correlation function along the phase director (parallel to the $C_{60}$[110] axis), showing the oscillations typical of the smectic phase at 600 K.

Already from the snapshot in **Figure 5**a, it appears that our attempt to obtain a liquid crystalline phase of T6 with planar alignment on $C_{60}$ was successful, with T6 molecules forming smectic layers extending from the bottom to the top surface. A further analysis of the phase director of the liquid crystal phase demonstrates that its orientation is templated by the surface, as it coincides with the $C_{60}$ [110] direction.

The fingerprint of a smectic phase is the presence of density fluctuations along the direction normal to the layers (parallel to $C_{60}$ [110] axis), that gives rise to a characteristic X-ray peak corresponding to the layer spacing $d$. The amplitude of the density fluctuations is mainly captured by the order parameter $\tau_1 = \left\langle \cos\left(2\pi r_{12}/d\right)\right\rangle$, which appears as the first coefficient in a cosine series expansion of the linear pair correlation function along the director:[62]

$$g(r_{12}) = 1 + 2\sum_{n=1}^{\infty} \tau_n^2 \cos\left(2\pi n r_{12}/d\right) \quad (2)$$

The smectic order parameter is equal to 0.45, clearly confirming the presence of a layered structure as suggested by the profile of $g(r_{12})$ plotted in Figure 5c. This value is lower than in bulk T6 at the same temperature (0.52 in another study)[28] indicating that the confinement partially disrupts the positional order along the director. Correspondingly, the layer spacing is measured to be $d$ = 26.7 Å here, versus the bulk value of 26.2 Å. The slightly larger spacing is probably due to the strong tendency to form an integer number of smectic layers in the finite simulation box, rather than an effect of the interface or confinement.

In view of understanding the electronic processes which may occur upon illumination of the sample, it is also useful to analyze the local variation of positional order when moving away from the interface. Actually, in the LC phase at 600 K at least two layers of molecules form at the interface with $C_{60}$, as can be evinced from the density profile in Figure 5b. A similar interfacial ordering effect has been previously observed for glassy quaterthiophene on fullerene[14] or for liquid crystals on atomically flat inorganic surfaces.[60,61] Such an increased structuring at the interface, which persists also at room temperature (vide infra), is likely to strongly affect charge separation kinetics and energetics.[9–11]

## 4. Analysis of the Structures at Room Temperature

Since organic electronics devices operate at room temperature, the vapor-deposited and the LC-annealed samples were equilibrated at 300 K prior to analyze in greater detail their morphology. In general, T6 forms layered structures characterized by close intermolecular distances within the layers and a tendency to herringbone packing. The interfacial structures

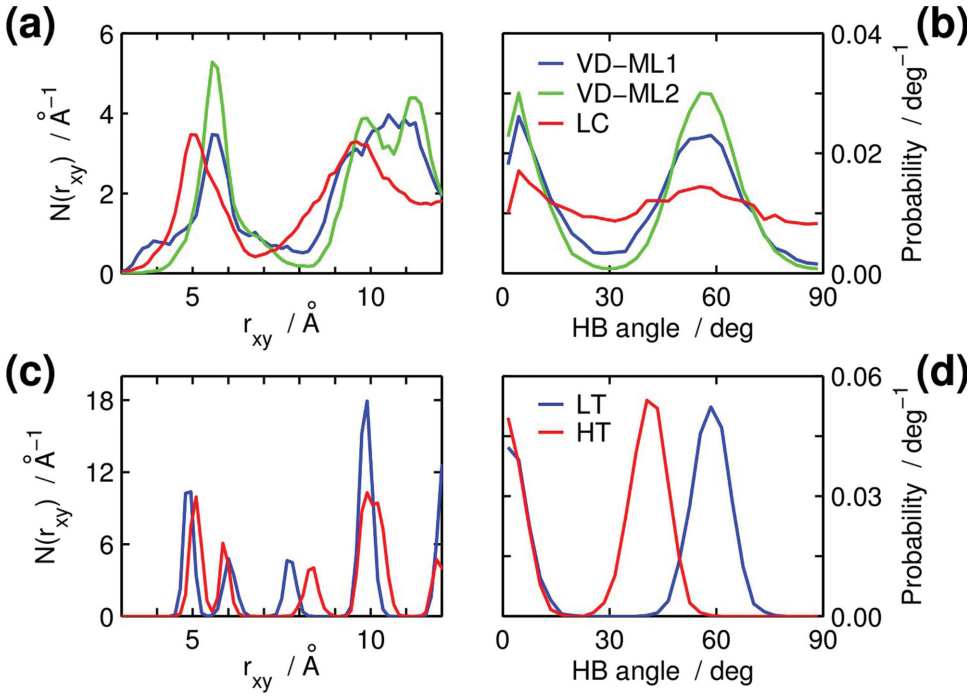


**Figure 6.** Density of neighbors $N(r_{xy})$ for T6 molecules in the layers (left, with $r_{xy}$ being the in-plane intermolecular distance) and of herringbone (HB) angles for the first six neighbors (right), calculated for the VD and LC-annealed sample (top), and the bulk T6 crystalline polymorphs (bottom). In both the VD and the LC-annealed samples at 300 K, the organization of T6 molecules presents the tendency to herringbone arrangements, with features of the $N(r_{xy})$ indicating that the T6 solid formed in both simulations is more similar to the high-temperature polymorph of T6.

obtained through different preparation conditions are here characterized, and their features compared to simulation results for bulk samples of the LT and HT polymorphs of T6.

The VD sample was first equilibrated at 300 K retaining the periodic boundary conditions as adopted in the deposition simulations; PBCs were then relaxed by completing the equilibration on an 2 × 2 enlarged $C_{60}$ substrate. Upon relaxing the constraint imposed by the simulation box, we notice a substantial rearrangement of the second and third monolayers, with molecules assuming a less tilted orientation, while negligible changes occur in ML1. We then discuss here the room-temperature structure obtained after relaxation of periodic boundary conditions (data relevant to the box-constrained system are reported in the Supporting Information).

The sample obtained by VD can be considered as a collection of independent crystalline monolayers: as discussed in the vapor growth section, there is no evidence for correlations between the tilting direction in the different MLs, with that of ML1 induced by the $C_{60}$ substrate. Conversely, proofs of spatial correlation within each ML can be found in the radial density of in-plane neighbors $N(r_{xy})$ (blue and green lines in **Figure 6**a), which shows a rather rich structuring, though not comparable with the corresponding one in the bulk crystal (Figure 6c). This function presents a single broad peak at short distance in ML1 ($r_{xy} \approx 5.7$ Å) and ML2 ($r_{xy} \approx 5.4$ Å), unlike in the bulk structures where two peaks corresponding to first and second nearest neighbors are resolved (see Figure 6c). The nearest-neighbor peak is broader for ML1 than for ML2, indicating a disordering effect of the $C_{60}$ substrate. The $N(r_{xy})$ distribution for ML3 is similar to that of ML2 (see Figure S7, Supporting Information).

The relative molecular orientations within the planes are characterized in terms of the distribution of the herringbone angles formed by the axes normal to the molecular planes of neighboring molecules (the six nearest neighbors are considered). The distribution for ML1 and ML2 in Figure 6b shows the two-peak structure characteristic of herringbone-packed molecular layers. The peak due to the four non-translationally equivalent neighbors gives an herringbone angle of ≈55–60 degrees. This value is similar to that of the LT polymorph (see Figure 6d), although the distributions of herringbone angles in the VD layers are broader than in the bulk structures. In order to characterize the positional order within the layers, it is necessary to separate the spatial correlations along two axes, and we perform that by means of the pair correlation function in the plane, $N(x,y)$, shown in **Figure 7**a,b for ML1 and ML2, respectively. The spots in the $N(x,y)$ allow us to extract the two-dimensional crystal cell parameters for each of the ML, whose values, along with those of the LT and HT bulk polymorphs, are reported in **Table 1**. A certain amount of structural disorder, inherited form the out-of-equilibrium vapor growth at 500 K, is present in the MLs, resulting again in much broader peaks in the $N(x,y)$ with respect to those of bulk samples, shown in Figure S9 (Supporting Information) for comparison.

Quite interestingly, the spread of the peaks of the $N(x,y)$ is strongly anisotropic for ML1, and is maximized along the $C_{60}[\bar{1}10]$ direction. A closer inspection of the $N(x,y)$ pattern reveals the formation of an ordered structure of T6 characterized by four molecules in the unit cell (green box in Figure 7a), unlike the typical (two-dimensional) cells that count two molecules. This is an epitaxial structure characteristic of T6 on

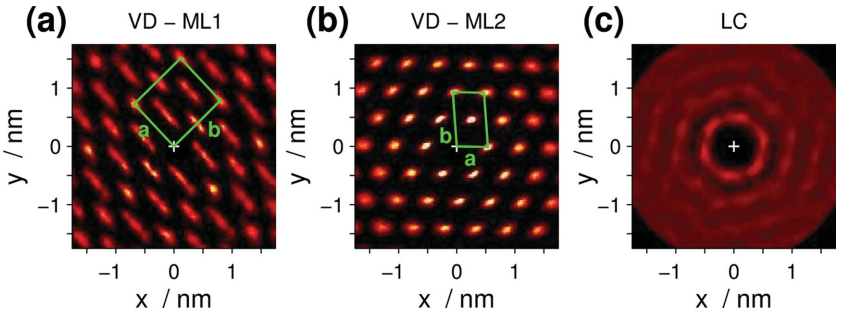


**Figure 7.** Distribution of the intra-layer intermolecular distances $N(x,y)$ for the first monolayer in a) ML1 and b) ML2 obtained by VD, and the respective in-plane unit cells (green frames). The cell of ML1 contains four molecules, against the two of ML2, because of the establishment of an epitaxial relationship with the $C_{60}$(001) facet. (c) $N(x,y)$ for the LC-annealed phase, for an arbitrary choice of in-plane axes. Note the relatively short-ranged hexagonal order of sample. All data are obtained from 300 K simulations.

$C_{60}$(001), in which the T6 cell vector *a* points along the $C_{60}$ direction and matches in length the distance between the grooves of the $C_{60}$ surface, that is, $\sqrt{2}a_{C_{60}} = 9.94$ Å (see Figure 1b). The epitaxial structure we observed in our simulation is ascribed to the periodic roughness of the $C_{60}$(001) facet, that, by modulating intermolecular distances, leads to the doubling of the T6 unit cell, and causes the anisotropic spots in the $N(x,y)$ in Figure 7a.

This epitaxial structure does not propagate to the subsequent MLs, whose $N(x,y)$ presents well-defined peaks characteristic of a structure with two molecules in the unit cell, as shown in Figure 7b for ML2. The cell obtained for ML2 and ML3, reported in Table 1, cannot be ascribed to none of the two bulk polymorphs, yet their parameters are closer to those of the HT one, as also confirmed by the $N(r_{xy})$ in Figure 6. Though in general the coexistence of different polymorphs is known to occur in T6 films, in particular at high deposition temperatures,[50] Radziwon and coauthors measured a terrace height ($c^*$ in Table 1) of about 23 Å for 100 nm-thick films of T6 grown on $C_{60}$,[44] thus typical of the LT polymorph and larger than the prediction of MD simulations for ML1, but very similar to the one for ML3.

Turning to the LC-annealed sample, the T6 phase can be considered as only partially crystalline, as it is characterized by interlayer positional and orientational order, inherited by the parent smectic phase, and a short-range order within the layers. A similar structure, though with standing T6 molecules, was obtained by Moser et al. by vacuum-depositing T6 on $SiO_2$ at high deposition rates.[63] By cooling the smectic to 300 K, the average sample density rises from 1.17 to 1.44 g/cm$^3$ and the orientational order parameter of T6 molecules increases from $<P_2>$ = 0.85 to 0.94. Moreover, upon cooling we have also observed the onset of a tilt of ≈20 degrees between the alignment direction and the layer planes, a feature that is characteristic of the crystalline structures of many rod-like molecules, and oligothiophenes in particular.[29]

The pair correlation function in the plane $N(x,y)$ for the LC annealed sample at 300 K, shown in Figure 7c, reveals in this case the presence of a weak hexagonal order between first neighbors, and effective cylindrical symmetry at larger distances. Consistently, the radial density of in-plane neighbors (red line in Figure 6a) reveals two well-defined coordination shells. In particular the peak of nearest neighbors is considerably broader that in the VD sample and extends to smaller distances, revealing the presence of a consistent amount of T6 dimers with face-to-face arrangement. The herringbone order is barely detectable in T6 layers, as confirmed by the rather flat distribution of herringbone angles in Figure 6b.

Finally, we consider the intramolecular degrees of freedom of T6, specifically focusing on the conformational disorder that may occur at finite temperature in virtue of the comparable energies of *trans* and *cis* inter-ring conformations and the small energy barrier between the two.[28] The lowest energy full-*trans* structure is largely the most abundant at room temperature (83% and 72% in VD and LC samples, respectively), though bent conformers with one *cis* torsion have appreciable populations (see Table S2, Supporting Information).

We conclude this section noticing that because of the sudden cooling underwent by our samples, unavoidable in computer simulations, our room-temperature structures are necessarily more disordered than real ones, especially in the case of the LC-annealed one, where the thermodynamic control over the final morphology is looser. However, part of this disorder is intrinsic to the processing conditions, and to the soft nature of organic materials and their interfaces. This disorder is expected to produce a larger spread of intermolecular electronic couplings and energy levels with respect to the respective bulk crystal phases, with possible important consequences on the electronic processes taking place at the heterojunction.

**Table 1.** Room-temperature parameters of the in-plane cell of T6. *a* and *b* are respectively the short and long axes in the plane. *a* (*b*) corresponds either to the axis *c* (*b*) of the original LT cell,[70] or to the axis *b* (*a*) of the original HT cell.[71] Lengths are given in Å, angles in degrees. The uncertainty on the cell parameters calculated for VD MLs is of 0.2 Å for distances and 3 degrees for angles.

| | | *a* | *b* | γ | tilt | *c** |
|---|---|---|---|---|---|---|
| LT | exp | 6.03 | 7.85 | 90 | 24.7 | 22.36 |
| LT | sim | 6.12 | 7.81 | 89.7 | 24.3 | 22.83 |
| HT | exp | 5.68 | 9.15 | 90 | 33.6 | 20.48 |
| HT | sim | 5.99 | 8.40 | 90.1 | 31.8 | 21.48 |
| VD-ML1 | sim | 10.0 | 11.2 | 89 | 39 | 19.1 |
| VD-ML2 | sim | 5.3 | 9.4 | 94 | 30 | 21.3 |
| VD-ML3 | sim | 5.7 | 8.9 | 92 | 26 | 22.1 |

## 5. Conclusions

We have studied in detail the molecular organization of the donor-acceptor system formed by a thin film of sexithiophene deposited on the crystal (001) facet of the n-type organic semiconductor $C_{60}$, by means of a molecular dynamics simulation technique that imitates the vapor deposition process. Following the growth of the first three monolayers of T6 we found that the first event is the formation of a wetting layer of T6 molecules, with their long axes lying flat aligned along the grooves formed

between rows of $C_{60}$ molecules along the ⟨110⟩ directions. By increasing the coverage, molecules gradually tilt away from the $C_{60}$ surface forming a crystalline monolayer of standing molecules. A commensurism with the two-dimensional lattice of $C_{60}$(001), leading to the formation of an epitaxial structure with four T6 molecules in the unit cell, was found. We observed the growth of the second and third monolayers to take place instead in three coverage-dependent steps: i) formation of disordered aggregates of flat-lying molecules at low coverage; ii) nucleation of islands of circular shape when the aggregate becomes larger than one hundred molecules, characterized by nearly standing and herringbone-packed molecules in the core region, and tilted molecule at the edges assuming a chiral, propeller-like, arrangement; iii) expansion of the island with gradual increase of the crystalline core size. This mechanism is broadly consistent with experimental observations of the growth of T6 on $C_{60}$,[44] as well as on the more widely investigated but chemically different $SiO_2$ substrate.[42,43,50] The mechanism we propose for the growth of T6 on T6, involving the formation of crystalline islands with chiral edges, is quite surprising, with its spontaneous symmetry breaking in the absence of screw dislocations in the support slab,[64] and different from what we previously found, e.g., for pentacene on $C_{60}$.[27]

We notice that the standing T6 morphology obtained by vapor deposition on $C_{60}$ is far from being optimal for solar cell applications, because it hampers the charge transport in the direction normal to the interface. On the other hand this disposition is not necessarily unique, as suggested by the initial planar orientation of the T6 molecules. We thus employed computer simulations to examine the effects of a thermal treatment of the film and we showed how the standing geometry could be turned in a completely different planar one by simply annealing the sample at 600 K so as to melt the T6 crystal in its smectic phase. In this mesophase T6 molecules tend to align flat on the $C_{60}$ surface and this configuration propagates easily across the whole sample. The smectic layers, extending in the direction perpendicular to the interface with $C_{60}$, are conserved also when the sample is cooled back to the room temperature crystal phase. The planar interface obtained should favor charge separation and an efficient two-dimensional charge transport. This specific example suggests that transforming one component from crystalline to its liquid crystalline state, if available, can produce dramatic effects on its orientation at the interface, and that those changes can be exploited for controlling the morphology of small molecule donor/acceptor interfaces.

In summary, the in silico investigation of organic crystal growth by means of out-of-equilibrium atomistic molecular dynamics provides a very insightful picture of the multi-step nature of this fundamental process, at a level of detail still not accessible to experiments, and can moreover suggest possibly viable strategies for tuning organic interfaces and improving their features.

## 6. Experimental Section

The atomistic force field for T6 and $C_{60}$, based on the AMBER parameterization[65] was developed and validated against experimental crystal structures and transition temperatures in previous works.[27,28] The same force field was used for calculating the mixed T6-C60 interactions, by adopting the standard Lorentz-Berthelot mixing rules. T6-C60 interaction profiles for selected bimolecular configurations computed with our force field and the recent long-range corrected density functional revPBE0-NL[66] (Orca code, version 3.0,[67] are shown in Figure S12 (Supporting Information). The satisfactory agreeement between the two methods validates the use of our force field for mixed interactions.

MD simulations were performed with the NAMD code (version 2.9),[68] employing a timestep of 1 and 2 fs for bonded and non-bonded interactions, respectively. Pair interactions were computed within a cutoff distance of 1.5 nm, and full electrostatic sums evaluated with the Particle Mesh Ewald algorithm every 4 fs. Periodic boundary conditions were applied, and temperature (pressure, where appropriate) control was achieved with a Berendsen thermostat (barostat) with a relaxation time of 10 ps (compressibility of $4.57 \times 10^{-5}$ $bar^{-1}$).

The vapor growth of T6 on $C_{60}$(001) was simulated as a series of non-equilibrium MD simulations of 200 ps, corresponding to the different deposition steps, performed at constant temperature and volume, with a scheme very similar to the one employed in another study[27] for depositing pentacene on $C_{60}$. The x and y box sizes were fixed to 98.364 Å in order to accommodate the $C_{60}$ substrate (a 2D crystalline slab obtained as a $7 \times 7 \times 2$ supercell of the experimental crystal structure,[69] while the size along the direction perpendicular to the interface ($z$) was set to 200 Å to allow a suitably large empty space for simulating the vapor deposition. The lower half of fullerene molecules are kept fixed to reduce the computational effort. During the deposition, temperature was set to 500 K, instead of the most obvious choice of 300 K, in order to accelerate the molecular motion without significantly changing the free energy landscape as T6 and $C_{60}$ are both crystalline at 500 K. Differently from the literature,[27] here we introduced at each step the incoming T6 molecule at 50 Å from the growing film, endowing it with an initial velocity of 2 Å/ps directed towards the $C_{60}$ surface. This procedure was iterated for 1030 steps. We then equilibrated the system at 300 K with a first 10 ns simulation, in which we used the same simulation box as in the deposition, followed by a 5 ns run, where the T6 cristallite was placed on a $2 \times 2$ replica of the $C_{60}$ substrate. The latter allowed relaxing the constraints imposed by periodic boundary conditions on the structure of T6 MLs.

The liquid crystal-annealed T6/$C_{60}$ sample, consisting of 1600 T6 and 760 $C_{60}$ (2D slab, $8 \times 8 \times 3$ supercell), was simulated at constant temperature and pressure (1 atm). The $C_{60}$ slab dimensions were chosen so as to allow the formation of an integer number of smectic layers, as preliminary simulations on smaller samples showed the tendency for a planar alignment of T6, with the phase director along the $C_{60}$[110] direction. This system was first annealed for 33 ns at 600 K (23 ns equilibration + 10 ns production) and then cooled down to 300 K and equilibrated for 16 ns, before running 9 ns of production.

## Supporting Information

Supporting Information is available from the Wiley Online Library or from the author.

## Acknowledgements

The research leading to these results has received funding from the European Commission Seventh Framework Programme (FP7/2007–2013) under Grant Agreement number 228424 Project MINOTOR. G.D. is currently supported by a FP7 Marie Curie BEIPD- COFUND Fellowship. The authors thank Prof. Aldo Brillante for many enlightening discussions and for carefully reading the manuscript.

Received: August 1, 2014
Revised: September 9, 2014
Published online: October 14, 2014

[1] *Organic Solar Cells. Materials and Device Physics*, (Ed: W. C. H. Choy), Springer-Verlag, Berlin **2013**.
[2] *Organic Photovoltaics. Mechanisms, Materials, and Devices*, (Eds: S.-S. Sun, N. S. Sariciftci) CRC Press, Taylor & Francis, London**2005**.
[3] J.-L. Bredas, J. E. Norton, J. Cornil, V. Coropceanu, *Acc. Chem. Res.* **2009**, *42*, 1691–1699.
[4] J. Cornil, S. Verlaak, N. Martinelli, A. Mityashin, Y. Olivier, T. Van Regemorter, G. D'Avino, L. Muccioli, C. Zannoni, F. Castet, D. Beljonne, P. Heremans, *Acc. Chem. Res.* **2013**, *46*, 434–443.
[5] S. R. Yost, T. Van Voorhis, *J. Phys. Chem. C* **2013**, *117*, 5617–5625.
[6] F. Castet, G. D'Avino, L. Muccioli, J. Cornil, D. Beljonne, *Phys. Chem. Chem. Phys.* **2014**, *16*, 20279-20290.
[7] T. W. Holcombe, J. E. Norton, J. Rivnay, C. H. Woo, L. Goris, C. Piliego, G. Griffini, A. Sellinger, J.-L. Brédas, A. Salleo, J. M. J. Fréchet, *J. Am. Chem. Soc.* **2011**, *133,* 12106–12114.
[8] D. N. Congreve, J. Lee, N. J. Thompson, E. Hontz, S. R. Yost, P. D. Reusswig, M. E. Bahlke, S. Reineke, T. Van Voorhis, M. A. Baldo, *Science* **2013**, *340,* 334–337.
[9] J. Idé, R. Méreau, L. Ducasse, F. Castet, H. Bock, Y. Olivier, J. Cornil, D. Beljonne, G. D'Avino, O. M. Roscioni, L. Muccioli, C. Zannoni, *J. Am. Chem. Soc.* **2014**, *136*, 2911–2920.
[10] Y. Yi, V. Coropceanu, J.-L. Bredas, *J. Mater. Chem.* **2011**, *21*, 1479–1486.
[11] H. Tamura, I. Burghardt, M. Tsukada, *J. Phys. Chem. C* **2011**, *115*, 10205–10210.
[12] G. D'Avino, S. Mothy, L. Muccioli, C. Zannoni, L. Wang, J. Cornil, D. Beljonne, F. Castet, *J. Phys. Chem. C* **2013**, *117*, 12981–12990.
[13] P. Clancy, *Chem. Mater.* **2011**, *23*, 522–543.
[14] S. Y. Reddy, Vikram K. Kuppa, *J. Phys. Chem. C* **2012**, *116*, 14873–14882.
[15] L. Muccioli, G. D'Avino, R. Berardi, S. Orlandi, A. Pizzirusso, M. Ricci, O. M. Roscioni, C. Zannoni, Supramolecular organization of functional organic materials in the bulk and at organic/organic interfaces: A modeling and computer simulation approach, in *Multiscale Modelling of Organic and Hybrid Photovoltaics*, Vol. *352* of *Topics in Current Chemistry*, (Eds: D. Beljonne, J. Cornil), Springer, Berlin–Heidelberg **2014**, pp 39–101.
[16] Y.-T. Fu, C. Risko, J.-L. Brédas, *Adv. Mater.* **2013**, *25*, 878–882.
[17] C. W. Tang, *Appl. Phys. Lett.* **1986**, *48*, 183–185.
[18] T. Ameri, G. Dennler, C. Lungenschmied, C. J. Brabec, *Energy Environ. Sci.* **2009**, *2*, 347–363.
[19] W. Cambarau, A. Viterisi, J. W. Ryan, E. Palomares, *Chem. Comm.* **2014**, *50*, 5349–5351.
[20] J. Halls, C. A. Walsh, N. C. Greenham, E. A. Marseglia, R. H. Friend, S. C. Moratti, A. B. Holmes, *Nature* **1995**, *376*, 498–500.
[21] G. Yu, J. Gao, J. C. Hummelen, F. Wudl, A. J. Heeger, *Science* **1995**, *270*, 1789–1791.
[22] S. Verlaak, D. Beljonne, D. Cheyns, C. Rolin, M. Linares, F. Castet, J. Cornil, P. Heremans, *Adv. Funct. Mater.* **2009**, *19*, 3809–3814.
[23] J. R. Tumbleston, B. A. Collins, L. Yang, A. C. Stuart, E. Gann, W. Ma, W. You, H. Ade, *Nat. Photonics* **2014**, *8*, 385–391.
[24] Y. Sun, G. C. Welch, W. L. Leong, C. J. Takacs, G. C. Bazan, A. J. Heeger, *Nat. Mat.* **2012**, *11*, 44–48.
[25] J. Roncali, P. Leriche, P. Blanchard, *Adv. Mater.* **2014**, *26*, 3821–3838.
[26] S. Sergeyev, W. Pisula, Y. H. Geerts, *Chem. Soc. Rev.* **2007**, *36*, 1902–1929.
[27] L. Muccioli, G. D'Avino, C. Zannoni, *Adv. Mater.* **2011**, *23*, 4532–4536.
[28] A. Pizzirusso, M. Savini, L. Muccioli, C. Zannoni, *J. Mater. Chem.* **2011**, *21*, 125–133.
[29] D. Fichou, *J. Mater. Chem.* **2000**, *10*, 571–588.
[30] F. Dinelli, M. Murgia, P. Levy, M. Cavallini, F. Biscarini, D. M. de Leeuw, *Phys. Rev. Lett.* **2004**, *92*, 116802.
[31] C. Simbrunner, *Semicond. Sci. Technol.* **2013**, *28*, 053001.
[32] Y. Ge, J. E. Whitten, *Chem. Phys. Lett.* **2007**, *448*, 65–69.
[33] J. Niederhausen, P. Amsalem, A. Wilke, R. Schlesinger, S. Winkler, A. Vollmer, J. P. Rabe, N. Koch, *Phys. Rev. B* **2012**, *86*, 081411.
[34] P. Amsalem, J. Niederhausen, A. Wilke, G. Heimel, R. Schlesinger, S. Winkler, A. Vollmer, J. P. Rabe, N. Koch, *Phys. Rev. B* **2013**, *87*, 035440.
[35] J. Sakai, T. Taima, K. Saito, *Org. Electron.* **2008**, *9*, 582–590.
[36] J. Sakai, T. Taima, T. Yamanari, K. Saito, *Sol. Energy Mater. Sol. Cells* **2009**, *93*, 1149–1153.
[37] N. Ishiyama, M. Kubo, T. Kaji, M. Hiramoto, *Org. Electron.* **2013**, *14,* 1793–1796.
[38] H. L. Zhang, W. Chen, L. Chen, H. Huang, X. S. Wang, J. Yuhara, A. T. S. Wee, *Small* **2007**, *3*, 2015–2018.
[39] L. Chen, W. Chen, H. Huang, H. L. Zhang, J. Yuhara, A. T. S. Wee, *Adv. Mater.* **2008**, *20*, 484–488.
[40] R. Wang, H. Y. Mao, H. Huang, D. C. Qi, W. Chen, *Appl. Phys. Lett.* **2011**, *109*, 084307.
[41] J. Wen, J. Ma, *Langmuir* **2010**, *26*, 5595–5602.
[42] M. A. Loi, E. Da Como, F. Dinelli, M. Murgia, R. Zamboni, F. Biscarini, M. Muccini, *Nat. Mater.* **2005**, *4*, 81–85.
[43] E. Da Como, M. A. Loi, M. Murgia, R. Zamboni, M. Muccini, *J. Am. Chem. Soc.* **2006**, *128*, 4277–4281.
[44] M. Radziwon, M. Madsen, F. Balzer, R. Resel, H.-G. Rubahn, *Thin Solid Films* **2014**, *558*, 165–169.
[45] D. Vanzo, M. Ricci, R. Berardi, C. Zannoni, *Soft Matter* **2012**, *8*, 11790–11800.
[46] F. R. Massaro, M. Moret, M. Bruno, D. Aquilano, *Cryst. Growth Des.* **2013**, *13*, 1334–1341.
[47] A. Brillante, I. Bilotti, R. G. Della Valle, E. Venuti, A. Girlando, *Cryst Eng Comm* **2008**, *10*, 937–946.
[48] S. L. Price, *Chem. Soc. Rev.* **2014**, *43*, 2098–2111.
[49] J.-F. Moulin, F. Dinelli, M. Massi, C. Albonetti, R. Kshirsagar, F. Biscarini, *Nucl. Instrum. Methods Phys. Res. Sect. B-Beam Interact. Mater. Atoms* **2006**, *246*, 122–126.
[50] A. Brillante, I. Bilotti, C. Albonetti, J.-F. Moulin, P. Stoliar, F. Biscarini, D. M. de Leeuw, *Adv. Funct. Mater.* **2007**, *17*, 3119–3127.
[51] A. Brillante, I. Bilotti, R. G. Della Valle, E. Venuti, A. Girlando, M. Masino, F. Liscio, S. Milita, C. Albonetti, P. D'Angelo, A. Shehu, F. Biscarini, *Phys. Rev. B* **2012**, *85*, 195308.
[52] M. Campione, S. Caprioli, M. Moret, A. Sassella, *J. Phys. Chem. C* **2007**, *111*, 12741–12746.
[53] G. Koller, S. Berkebile, J. R. Krenn, F. P. Netzer, M. Oehzelt, T. Haber, R. Resel, M. G. Ramsey, *Nano Lett.* **2006**, *6*, 1207–1212.
[54] S. Trabattoni, M. Moret, M. Campione, L. Raimondo, A. Sassella, *Cryst. Growth Des.* **2013**, *13*, 4268–4278.
[55] C. Taliani, R. Zamboni, G. Ruani, S. Rossini, R. Lazzaroni, *J. Mol. Electron.* **1990**, *6*, 225.
[56] S. Destri, M. Mascherpa, W. Porzio, *Adv. Mater.* **1993**, *5*, 43–45.
[57] S. Kuiper, W. F. Jager, T. Dingemans, S. J. Picken, *Liq. Cryst.* **2009**, *36*, 389–396.
[58] M. Dohr, O. Werzer, Q. Shen, I. Salzmann, C. Teichert, C. Ruzié, G. Schweicher, Y. H. Geerts, M. Sferrazza, R. Resel, *Chem. Phys. Chem.* **2013**, *14*, 2554–2559.
[59] J. Hanna, A. Ohno, H. Iino, *Thin Solid Films* **2014**, *554*, 58–63.
[60] A. Pizzirusso, R. Berardi, L. Muccioli, M. Ricci, C. Zannoni, *Chem. Sci.* **2012**, *3*, 573–579.
[61] O. M. Roscioni, L. Muccioli, R. G. Della Valle, A. Pizzirusso, M. Ricci, C. Zannoni, *Langmuir* **2013**, *29*, 8950–8958.
[62] M. F. Palermo, A. Pizzirusso, L. Muccioli, C. Zannoni, *J. Chem. Phys.* **2013**, *138*, 204901.
[63] A. Moser, I. Salzmann, M. Oehzelt, A. Neuhold, H.-G. Flesch, J. Ivanco, S. Pop, T. Toader, D. R. T. Zahn, D.-M. Smilgies, R. Resel, *Chem. Phys. Lett.* **2013**, *574*, 51–55.
[64] J. Venables, *Introduction to Surface and Thin Film Processes*, Cambridge University Press, Cambridge, UK **2000**.

[65] W. D. Cornell, P. Cieplak, C. I. Bayly, I. R. Gould, K. M. Merz Jr., D. M. Ferguson, D. C. Spellmeyer, T. Fox, J. W. Caldwell, P. A. Kollman, *J. Am. Chem. Soc.* **1995**, *117*, 5179–5197.
[66] J. C. Sancho-Garcia, Y. Olivier, *J. Chem. Phys.* **2012**, *137*, 194311.
[67] F. Neese, *Wiley Interdiscip. Rev.-Comput. Mol. Sci.* **2012**, *2*, 73–78.
[68] J. C. Phillips, R. Braun, W. Wang, J. Gumbart, E. Tajkhorshid, E. Villa, C. Chipot, R. D. Skeel, L. Kale, K. Schulten, *J. Comput. Chem.* **2005**, *26*, 1781–1802.
[69] P. A. Heiney, J. E. Fischer, A. R. McGhie, W. J. Romanow, A. M. Denenstein, J. P. McCauley Jr., A. B. Smith, D. E. Cox, *Phys. Rev. Lett.* **1991**, *66*, 2911–2914.
[70] G. Horowitz, B. Bachet, A. Yassar, P. Lang, F. Demanze, J.-L. Fave, F. Garnier, *Chem. Mater.* **1995**, *7*, 1337–1341.
[71] T. Siegrist, R. M. Fleming, R. C. Haddon, R. A. Laudise, A. J. Lovinger, H. E. Katz, P. Bridenbaugh, D. D. Davis, *J. Mater. Res.* **1995**, *10*, 2170–2173.